European Journal of Medicinal Chemistry 78 (2014) 157–166

Contents lists available at ScienceDirect

European Journal of Medicinal Chemistry

journal homepage: http://www.elsevier.com/locate/ejmech

Original article

Fluorinated benzophenone derivatives: Balanced multipotent agents for Alzheimer's disease

Federica Belluti [a,*], Angela De Simone [b], Andrea Tarozzi [b], Manuela Bartolini [a], Alice Djemil [b], Alessandra Bisi [a], Silvia Gobbi [a], Serena Montanari [a], Andrea Cavalli [a,c], Vincenza Andrisano [b], Giovanni Bottegoni [c], Angela Rampa [a]

[a] Department of Pharmacy and Biotechnology, University of Bologna, Via Belmeloro 6, 40126 Bologna, Italy
[b] Department for Life Quality Studies, Alma Mater Studiorum, University of Bologna, Corso d'Augusto 237, 47900 Rimini, Italy
[c] Department of Drug Discovery and Development, Istituto Italiano di Tecnologia, Via Morego 30, 16163 Genova, Italy

ARTICLE INFO

Article history:
Received 29 September 2013
Received in revised form
12 March 2014
Accepted 14 March 2014
Available online 16 March 2014

Keywords:
Acetylcholinesterase
Alzheimer's disease
Antioxidant activity
BACE-1
Benzophenone
Drug design
Lead identification

ABSTRACT

In an effort to develop multipotent agents against β-secretase (BACE-1) and acetylcholinesterase (AChE), able to counteract intracellular ROS formation as well, the structure of the fluorinated benzophenone **3** served as starting point for the synthesis of a small library of 3-fluoro-4-hydroxy- analogues. Among the series, derivatives **5** and **12**, carrying chemically different amino functions, showed a balanced micromolar potency against the selected targets. In particular, compound **12**, completely devoid of toxic effects, seems to be a promising lead for obtaining effective anti-AD drug candidates.

1. Introduction

Alzheimer's disease (AD) is a devastating neurodegenerative disorder that accounts for the majority of cases of dementia. It afflicts over 30 million people worldwide and these figures are expected to quadruple by 2050. At present, the only available treatments treat the symptoms of AD. Affecting neurotransmission by means of inhibitors of acetylcholinesterase (AChE), a well known molecular target involved in AD pathology, and N-methyl-D-aspartate (NMDA) receptor antagonists, makes it possible to slow down the cognitive decline associated with AD, yet showing only modest palliative clinical efficacy without affecting the disease progression or correcting the neurodegenerative process. In the last few years, this lack of an effective cure has fuelled an intense search for disease-modifying agents that, by targeting the underlying pathophysiology of AD, could control the disease process and slow down its clinical course [1]. In this scenario, the development of multitarget agents, chemical entities able to simultaneously modulate multiple biological targets significantly involved in AD neurotoxic pathway, has clearly emerged as a successful strategy [2].

A key event in AD pathogenesis is the accumulation of amyloid-β (Aβ) peptide in the brain. The $A\beta_{42}$ monomers aggregate into toxic extra-cellular oligomeric species, which, in turn, form insoluble fibrillar aggregates, that compose the core of the dense amyloid plaques [3,4]. These structures insert themselves into neuronal membranes and induce lipid peroxidation, protein oxidation and increased production of reactive oxygen species (ROS) and reactive nitrogen species (RNS), together with loss of function of many antioxidant defence enzymes, thus contributing to oxidative stress and neurotoxicity [5,6]. A common concept of the amyloid cascade hypothesis is that the aggregation of $A\beta_{42}$ peptide into toxic fibrils is the main initiating event that sets off a cascade of neurobiological processes, such as neurotoxicity, oxidative damage and

Abbreviations: AChE, acetylcholinesterase; AD, Alzheimer's disease; ABP, aminobenzylpiperidine; Aβ, amyloid-β; APP, amyloid precursor protein; BACE-1, β-secretase; CNS, central nervous system; HE, hydroxyethylene; FRET, fluorescence resonance energy transfer; PDB, protein data bank; ROS, reactive oxygen species; SAR, structure–activity relationships; *t*-BuOOH, *tert*-butylhydroperoxide.

* Corresponding author.
E-mail address: federica.belluti@unibo.it (F. Belluti).

http://dx.doi.org/10.1016/j.ejmech.2014.03.042
0223-5234/

inflammation, ultimately culminating with extensive brain atrophy, neuronal dysfunction, and cognitive decline [7]. The central nervous system (CNS) accumulation of unbound transition metals, such as iron and copper, has also been considered a significant source of oxidant species [8]. Recent *in vivo* studies demonstrated the presence of Aβ in mitochondrial membranes, where it was thought to be responsible for both the disruption of the electron transport chain and the irreversible cell damage [9]. All these factors are not independent of each other, and it is plausible that, especially in the early stages of the disease process, Aβ could enter the mitochondria where it would increase the generation of ROS and induce oxidative stress. Hence, the "oxidative stress hypothesis" states that the increased production of free radicals in AD is a potential target for therapeutic strategies; as such, therapeutic modalities involving antioxidants may be an effective approach to the treatment of this neurodegenerative disease [10].

Aβ is generated by the proteolytic processing of a larger membrane-bound precursor protein, known as the amyloid precursor protein (APP), upon sequential cleavage by two aspartyl proteases, β-secretase (also known as β-site APP cleaving enzyme-1, or BACE-1) and γ-secretase. It has been demonstrated that a variety of stress factors, including hypoxia, ischaemic injury and inflammation, can induce BACE-1 expression in experimental models of sporadic AD [11–14]. In particular, recent studies support the hypothesis that oxidative stress, secretase function and Aβ production are strictly interrelated events and suggest that inhibition of BACE-1 may have a synergic therapeutic effect with antioxidant compounds [10,11,15]. In this context, novel multipotent agents against BACE-1 and oxidative stress have gained attention for their potential as effective anti-AD drug candidates. The first generation of BACE-1 inhibitors focused on compounds with a peptide or peptidomimetic structure, designed as transition-state (TS) mimetics, and different substrate models were designed to closely interact with the BACE-1 catalytic aspartic acids (Asp 32 and Asp 228, catalytic dyad) [16] such as OM99-2, a 8-aminoacid residue hydroxyethylene (HE)-based analogue that spans the P4 to P4′ binding pockets of BACE-1, showing a noteworthy hydrogen bonding network within the active site, together with a direct interaction among the OH of the HE function and the catalytic dyad. Notwithstanding its nanomolar inhibitory potency, this compound showed suboptimal *in vivo* pharmacokinetics and low brain penetration [17]. Generally, the majority of the early BACE-1 inhibitors were characterized by complex, high molecular weight structural motifs, lacking drug-like properties [18]. Since the first X-ray crystal structures of BACE-1 were reported, intensive efforts have focused on the development of potent enzyme inhibitors that possess ideal properties such as oral bioavailability and a good pharmacokinetic profile [17]. The identification of small molecule inhibitors of BACE-1 with CNS permeability represents an important and difficult challenge since, in order to mediate brain Aβ lowering, inhibitors ought to be able to cross the blood–brain barrier (BBB) [19]. A 3-D pharmacophore map of BACE-1 has also been proposed, to guide the design and optimization of inhibitors [20]. Currently, several crystal structures of the catalytic domain of BACE-1, alone or in complex with an inhibitor, have been deposited in the Protein Data Bank (PDB). The structural information that emerged from these studies was employed for structure-based drug discovery projects, leading to the identification of several classes of non-peptidic BACE-1 inhibitors with novel core templates and with improved pharmacokinetics profile [16,18,21].

2. Design

In a drug discovery effort to obtain single multitarget small molecules as anti-AD drug candidates, we further investigated the potential of the benzophenone core structure to hit several targets involved in AD. This scaffold has indeed proved to be a privileged structure, a versatile pharmacophore nucleus, that could be exploited through suitable modifications to provide ligands for an array of biological targets [22,23]. Benzophenone has recently been employed by the authors as a starting point for obtaining compounds able to modulate the actions of AChE [24,25]. Following a previous research project aimed at identifying new chemical entities able to inhibit both BACE-1 and AChE enzymes [26], our internal benzophenone-based collection of AChE inhibitors, bearing a *N,N′*-benzylmethylamine function to target the catalytic binding site of the enzyme, was screened against BACE-1. Given that the cyclic amines proved to be suitable for specific hydrogen bonding with the catalytic aspartic acid, this tertiary amine function could hold promise for interacting with the enzyme, improving the compound solubility as well. Among the tested compounds, derivatives **1**–**4**, with AChE inhibition values ranging from sub-micro to low micromolar (Table 1), showed a promising trend of BACE-1 inhibition, that made it possible to gain insight into the benzophenone substitution pattern essential for this enzyme. Compound **1**, with a 3,4-dimethoxy benzophenone nucleus, endowed with sub-micromolar AChE inhibitory potency [24], when tested at 5 μM concentration showed low BACE-1 inhibition (20%). Removal of the methoxy group in position 3 (compound **2**) led to a notable decrease in potency. Interestingly compound **3**, with a fluorine atom instead of the 3-methoxy substituent, was identified as a weak BACE-1 inhibitor (10.72% of inhibition at 3.38 μM concentration). Notwithstanding its poor activity against BACE-1, compound **3** might be interesting from a pharmacokinetic perspective, since the presence of a fluorine substituent on an aromatic ring could impart a variety of properties, including enhanced binding interactions, metabolic stability, and selective reactivity [27]. For these reasons, **3** could be regarded as a hit compound to be further modified to obtain more potent analogues, and given that the strongly electron withdrawing effect of the fluorine atom markedly influences the acidity of neighbouring functional groups, we then synthesized the corresponding des-methyl analogue **5** (Table 2). Gratifyingly, this compound was able to potently inhibit BACE-1, with an IC_{50} value in the low micromolar range, providing a five-

Table 1
*h*BACE-1 and *h*AChE inhibition profiles of compounds **1**–**4**.

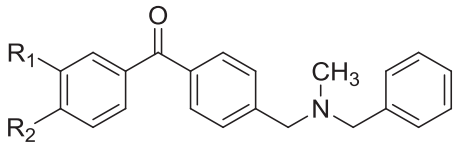

Cmpd	R_1	R_2	*h*BACE-1 inhibition (%)[a,b]	*h*AChE inhibition[b,c] IC_{50} (μM) ± SEM
1	OCH_3	OCH_3	20 (at 5 μM)	0.46 ± 0.04
2	H	OCH_3	n.i.[d]	1.82 ± 0.08
3	F	OCH_3	10.72 (at 3.38 μM)	1.57 ± 0.08
4	H	OH	n.i.[d]	2.10 ± 0.09

[a] % inhibition of BACE-1 activity at the reported concentration of the tested compounds.
[b] Values are mean of two independent measurements, each performed in triplicate.
[c] See Refs. [24,25]. IC_{50} values represent the concentration of inhibitor required to decrease enzyme activity by 50% IC_{50} values were determined by following Ellman's method.
[d] n.i.: not inhibiting up to 4 μM.

Table 2
*h*BACE-1 inhibition profiles of compounds **5**–**15**.

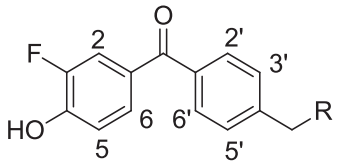

Cmpd	R	*h*BACE-1	
		Inhibition (%) at 3 μM[a,b] ± SEM	IC_{50} (μM)[b] ± SEM
5	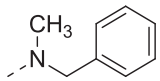	40.75 ± 1.05	3.66 ± 0.29
6	H	35.38 ± 4.09	
7	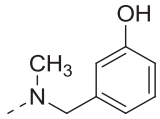	n.i.[c]	
8	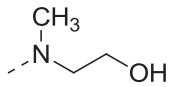	46.69 ± 5.12	
9	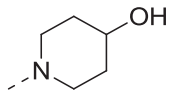	32.78 ± 4.06	
10	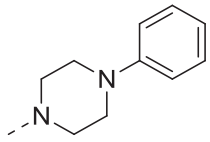	n.i.[c]	
11	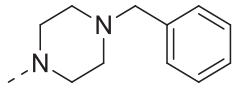	n.i.[c]	
12	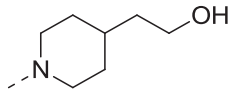	58.72 ± 3.22	2.32 ± 0.44
13	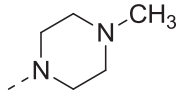	n.i.[c]	
14	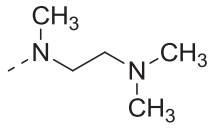	13.50 ± 5.50	
15	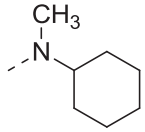	36.16 ± 3.05	
tacrine (THA)		n.i. (at 5 μM)[d]	
bis-(7)- THA		27.2 ± 0.2 (at 10 μM)	7.5 ± 0.4[d]

[a] % inhibition of BACE-1 activity (at 3 μM concentration) of the tested compounds.
[b] Values are mean ± SEM of two independent measurements, each performed in triplicate. SEM = standard error of the mean.
[c] n.i.: not inhibiting up to 4 μM.
[d] See Ref. [45].

fold enhancement in activity over **3** and being more active than the standard bis(7)-tacrine, which displayed an IC_{50} of 7.5 μM.

The pivotal importance of the fluorine substituent on BACE-1 inhibition was underlined by the finding that its removal (**4**) resulted in a loss of activity. **5** was docked into the active site of BACE-1 (Fig. 2A) to validate its capability to interact with key residues such as the catalytic dyad (see the Computational Studies paragraph for further details). As expected, the *N*,*N*′-benzylmethylamine portion turned out to be oriented towards the centre of the BACE-1 binding pocket by contacting the catalytic Asp 32 by means of electrostatic and H-bond interactions. Moreover, the 3-fluoro-4-hydroxybenzophenone framework established essential interactions at the S_2' subsite, interacting with the side chains of Tyr71, Tyr198, and Arg128, and to validate the impact of this molecular fragment on BACE-1 inhibition, the simplified analogue (**6**), lacking the *N*,*N*′-benzylmethylamine moiety, was tested. Inhibition data, listed in Table 2, were in agreement with the previous docking simulation performed on **5**, since the compound retained a somewhat good activity (35.38% inhibition at 3.0 μM), although lower relative to the lead **5**, and supported the presence of an appropriate tertiary amine function for obtaining effective BACE-1 inhibitors. The 3-fluoro-4-hydroxy-benzophenone nucleus, identified as an essential chemical feature for the binding within the BACE-1 enzyme, due to its good synthetic accessibility and low molecular weight (MW ~ 230) turned out to be an appropriate synthon for performing a parallel chemical synthesis; in particular, the methyl group could provide the insertion point for the amino group. With this idea we generated a small library of 3-fluoro-4-hydroxy-benzophenone-based compounds (**7**–**15**) in which the *N*,*N*′-benzylmethylamine group (R, Table 2) was replaced with a number of tertiary amines bearing different functional groups and flexible chains at the tertiary nitrogen atom, with the aim of performing a quick SAR study and of effectively determining the essential features of the R moiety required for an optimal interaction with the BACE-1 binding pocket.

3. Chemistry

The synthetic route followed for the preparation of the benzophenone derivatives (**5**–**15**) is depicted in Scheme 1. Intermediates **16** and **17** were synthesized according to a previously described procedure [24]. Cleavage of the methoxy group of **17** was accomplished by treatment with BBr_3 to obtain the key intermediate **18**, that was then subjected to nucleophylic attack by different amines to give, in parallel, the final compounds.

4. Biology

The benzophenone-based analogues presented in this study were first evaluated to investigate the ability to inhibit BACE-1 enzyme activity, by means of a biochemical assay performed using the fluorescence resonance energy transfer (FRET) methodology. FRET assay is based on the use of synthetic peptides carrying a fluorophore (donor group) and a quencher (acceptor group) bearing the Swedish mutated sequence of APP (-Leu ~ Asp- instead of Met ~ Asp) as substrate. The substrate becomes highly fluorescent upon enzymatic cleavage and the increase in fluorescence is linearly related to the rate of proteolysis. The methoxycoumarin based peptide M-2420 was used to evaluate enzyme inhibition by measuring the loss of fluorescence due to the presence of test compounds [28]. In particular, compounds **6**–**15** were tested at a concentration of 3 μM and their BACE-1 inhibition percentages are reported in Table 2. The IC_{50} values of the most active compounds (**5** and **12**) were determined by using the linear regression parameters. Subsequently, to determine the multitarget profile of **5**

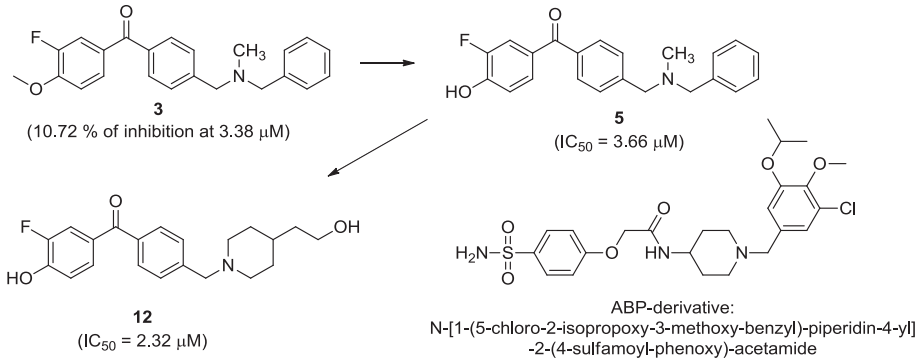

Fig. 1. Benzophenone BACE-1 inhibitors fragment evolution (inhibitory activities are reported in brackets), and structure of the ABP-based derivative employed for the computational studies.

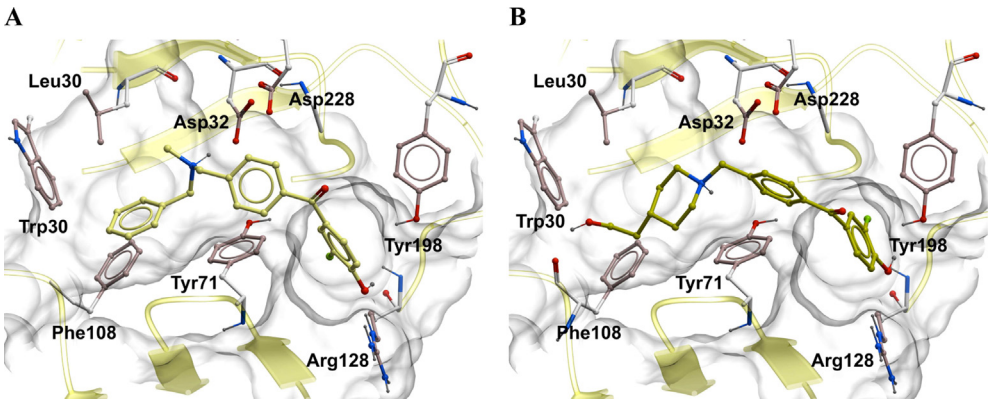

Fig. 2. The binding mode of **5** and **12** at the binding site of BACE-1. A) The bound conformation of **5** (carbon atoms in yellow). B) The bound conformation of **12** (carbon atoms in green). Residues of the binding site making relevant interactions are reported and labelled explicitly. (For interpretation of the references to colour in this figure legend, the reader is referred to the web version of this article.)

and **12**, we investigated their capability to inhibit the activity of human recombinant AChE by means of Ellman's method [29].

Finally, the antioxidant activity of **5** and **12** was evaluated against ROS formation in human neuronal SH-SY5Y cells following exposure to *t*-BuOOH or $A\beta_{25-35}$ peptides, the toxic core of Aβ, using compound **3** as a negative reference compound. In particular, the *t*-BuOOH is an organic peroxide that generates a pattern of ROS similar to that involved in the oxidative stress induced by Aβ [30]. In the same cells the neurotoxicity of the compounds was also determined.

5. Results and discussion

5.1. BACE-1 inhibition

Having established one of the important features required for BACE-1 inhibition, and in order to both explore the chemical space of the target and enhance the binding affinity of the designed 3-fluoro-4-hydroxybenzophenone framework, different R portions were introduced on this scaffold. BACE-1 inhibition data are reported in Table 2. The presence of additional hydroxyl and amino

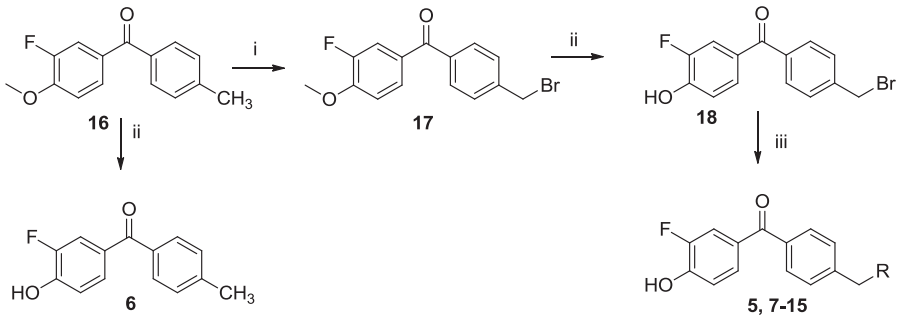

[a]Reagents and conditions: i) NBS, $(PhCOO)_2O$, CCl_4, reflux; ii) BBr_3; DCM, r.t.; iii) selected amine, TEA, toluene, reflux.

Scheme 1. Reagents and conditions: i) NBS, $(PhCOO)_2O$, CCl_4, reflux; ii) BBr_3; DCM, r.t.; iii) selected amine, TEA, toluene, reflux.

groups might make it possible to form favourable interactions with residues of the S_1 subsite. With this strategy in mind, we attempted to modify the electronic and hydrophobic/hydrophilic properties of the R portion. The effect of the introduction of a hydroxy appendage on the benzyl function was investigated with derivative **7**; this modification was not tolerated since no inhibition was detected at the tested concentration of 3 μM. In this case the substituent would alter the geometry of the designed molecule, thus hampering the interaction of the tertiary nitrogen with Asp 32 of the enzyme. The contribution of an alcohol function on the R portion was also evaluated with a subset of compounds (**8**, **9**, and **12**). In this regard, analogue **8**, bearing a 2-methylaminoethanol function, proved to be more active in comparison with the corresponding conformationally constricted piperidin-4-ol derivative **9** (46.69 and 32.78% of inhibition, respectively). A gain in potency with respect to **8** was achieved with compound **12**, bearing a 2-piperidin-4-ylethanol function, that proved to inhibit BACE-1 to a good extent (58.72%, $IC_{50} = 2.32$ μM), showing potency comparable to that of the lead **5**. On these bases, we assumed that this flexible moiety could play a crucial role, allowing an appropriate docking of the new compound into the BACE-1 binding site. In an attempt to support this hypothesis, a computational study performed on **12** showed that this R portion appears to be able to efficiently interact with the S_1 subsite (Fig. 2B; see the Computational Studies paragraph for further details). To probe the effects of an additional protonable nitrogen atom on the R portion, compounds **10**, **11**, and **13**, carrying different substituted piperazine moieties, were synthesized, but this functional group alteration was detrimental for the activity. A slight gain in potency, in comparison to the conformationally restricted methylpiperazine derivative analogue (**13**), was obtained with the corresponding 'open' analogue **14**, carrying a dimethylaminoethylmethylamino side chain (13.50% inhibition). Finally, analogue **15**, bearing a cyclohexylmethyl amine group, showed the same potency as the simplified 3-fluoro-4-hydroxy-4′-methylbenzophenone **6** confirming that the amino function could lead to a conformational modification that hampers the interaction with the enzyme residues.

5.2. Computational studies

To understand how our benzophenone-based derivatives inhibit BACE-1 enzyme, computational studies were performed on **5** and **12**. We carried out docking simulations modelling the binding site of BACE-1 according to the geometry displayed in the crystallographic complex with an aminobenzylpiperidine-based (ABP) BACE-1 inhibitor bearing a 3-sulfonamidephenoxy substituent (Fig. 1). X-ray crystal structure coordinates have been deposited in the PDB as entry 2ZJM (PDBid code: 2ZJM) [31]. This specific rearrangement of the enzyme was selected because this ABP derivative turned out to most closely match the pharmacophoric features of the selected compounds, among the 160 co-crystallized inhibitors available at the time these calculations were carried out (see Supporting Information for details). The putative bound conformation of **5** is reported in Fig. 2A. The 3-fluoro-4-hydroxybenzophenone group binds at the S_2' subsite interacting with the side chains of Tyr71, Tyr198, and Arg128 [32]. In particular, the 4-hydroxy group directly interacts with the side chain of Arg128. The basic nitrogen of the benzylmethylamine group establishes a hydrogen bond interaction with the outer oxygen of Asp 32, in the catalytic dyad. Finally, the benzylmethylamine group points toward the S_1 subpocket binding the hydrophobic region described by the side chains of Tyr71, Phe108, and Trp115. The docking of **12** with respect to the BACE-1 key residues is depicted in Fig. 2B, in which the benzophenone scaffold shows the same interaction pattern as that observed for **5**, whilst the piperidinethanol function appears flexible enough to efficiently bind at the S_1 subsite and establish a hydrogen bond with the backbone of Phe108. The proposed binding modes are in fairly good agreement with the reported activities for the other members of the library.

5.3. AChE inhibition

The ability of the newly synthesized compounds to inhibit human AChE catalytic activity was also investigated. Interestingly, only the most potent BACE-1 inhibitors of the series (**5** and **12**) proved to be weak inhibitors of AChE, with IC_{50} values in the low micromolar range (7.00 and 2.52 μM, respectively) less active than tacrine ($IC_{50} = 0.25$ μM). The remaining molecules showed only a slight ability to inhibit human AChE (data not shown).

5.4. Antioxidant activity and neurotoxicity in human neuronal SH-SY5Y cells

We evaluated the ability of compounds **3**, **5** and **12** to counteract intracellular ROS formation evoked by *t*-BuOOH (100 μM) and $A\beta_{25-35}$ peptides (5 μM) in human neuronal SH-SY5Y cells using DHE assays. As shown in Fig. 3, compounds **5** and **12**, but not **3**, significantly inhibited the ROS formation elicited by both *t*-BuOOH and $A\beta_{25-35}$ peptides in SH-SY5Y cells at concentrations of 3 μM and 5 μM. In particular, the maximum inhibition of ROS formation elicited by $A\beta_{25-35}$ peptides was 30% for both compounds **5** and **12**. In similar experimental conditions, the well-known antioxidant N-Acetylcysteine (500 μM) decreases ROS formation by 35% (data not shown). In parallel, the neurotoxicity of the same compounds in SH-SY5Y cells was then evaluated by the reduction of MTT to formazan. The persistent treatment of SH-SY5Y cells with **5**, but not **3** and **12**, significantly decreased the neuronal viability at higher concentrations of 10 and 50 μM (Fig. 4). Taken together, these results suggest that the des-methylation of **3** contributes to give **5** and **12** antioxidant properties. In particular, the presence of hydroxy groups bound to the aromatic ring could explain the ability of both compounds to counteract ROS formation at neuronal level. Interestingly, the affected neuronal viability recorded with **5**, bearing a *N*,*N*′-benzylmethylamine moiety, can be overcome with the 2-(piperidin-4-yl) ethanol function present in **12**.

6. Conclusions

In this paper, a new series of small molecules based on the 3-fluoro-4-hydroxybenzophenone core structure was developed to obtain BACE-1 inhibitors. This main framework was identified upon a structural modification performed on the weak BACE-1 inhibitor **3**, devoid also of antioxidant activity. The resulting compound **5** showed a remarkable change in the biological profile, such as a noteworthy gain in both BACE-1 inhibition and antioxidant activity. Computational studies confirmed that the 3-fluoro-4-hydroxy substitution pattern of the benzophenone scaffold seemed to be suitable for interactions with the biological counterpart. Moreover, the presence of a protonable tertiary nitrogen atom, having the capability to establish H-bonds with a catalytic aspartate, further reinforced the BACE-1 binding. In this respect, the nature of the substituent on this atom strongly influenced the capability to inhibit the enzyme. Among the novel derivatives, compounds **5** and **12**, albeit carrying chemically different amine functions, showed comparable potencies against the selected targets (balanced inhibitory potencies). In particular, they proved to be able to inhibit human recombinant BACE-1 enzyme to a good extent (low μM range) and the same was observed for the inhibition of human AChE and for antioxidant activity in human neuronal SH-SY5Y cells.

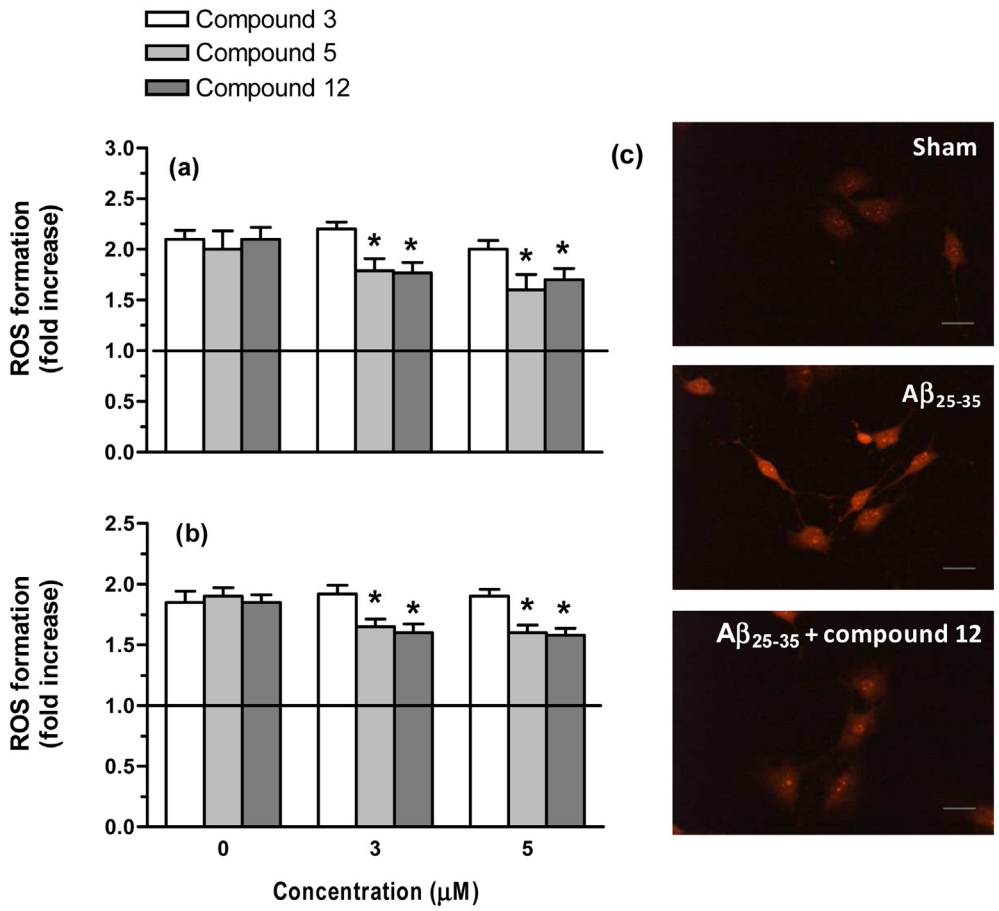

Fig. 3. Antioxidant activity of compounds **3**, **5** and **12** in SH-SY5Y cells. (a) SH-SY5Y cells were co-treated with various concentrations of compounds and *t*-BuOOH (100 μM) for 30 min. (b) SH-SY5Y cells were co-treated for 3 h with various concentrations of compounds and $A\beta_{25-35}$ peptides (5 μM). At the end of incubation, intracellular ROS formation was determined using the probe DHE (as described in the experimental section). The results obtained are expressed as fold increases of ROS formation induced by exposure to *t*-BuOOH or $A\beta_{25-35}$ peptides. The values are shown as mean ± SD of three independent experiments (*$P < 0.05$ vs. untreated cells at ANOVA with the Dunnett post hoc test). (c) Representative images of ROS formation induced by $A\beta_{25-35}$ peptides. Scale bars: 100 μm.

It is noteworthy that the overload of ROS induces accumulation of Aβ, establishing a vicious circle that reinforces the oxidative stress with strengthening of oxidative damage at neuronal level [33].

Moreover, since final targets of this study are located in the CNS, the possibility for the designed compounds to penetrate the BBB was also estimated by calculation of molecular lipophilicity, a physico-chemical property well known to influence BBB penetration. In particular, logP values were predicted by means of ChemBioDraw Ultra 12.0 and proved to be ≤5 (4.69 and 3.24 for compounds **5** and **12**, respectively). With a number of hydrogen bond donors ≤3 (n. H-bond donors = 1 and 2 for compounds **5** and **12**, respectively), number of hydrogen bond acceptors largely below 7 (n. H-bond acceptors = 2 for both compounds), and molecular weights below 400 g/mol (349.40 and 357.42 g/mol for compounds **5** and **12**, respectively), the physico-chemical properties profiles of **5** and **12** are in compliance with Lipinski's and Wenlock's guidelines for good passive CNS penetration [34,35].

Given that AChE, BACE-1 and oxidative stress have been recognized to play a pivotal role for both onset and progression of AD, the development of non-peptidic small molecules able to inhibit these enzymes, and to tackle the oxidative stress, is a challenging area of drug discovery. Recent clinical studies suggest that the efficacy of β-secretase inhibitors has a better chance to be observed in the treatment of the early stages of AD [36]. During the progression of AD, secondary pathological events not directly induced by Aβ, such as neuroinflammation and oxidative stress, may provide a high background cognitive influence and obscure the benefit of Aβ reduction [37]. In this context, the use of β-secretase inhibitors with added antioxidant properties could extend their therapeutic window to the intermediate and late stages of AD. It is noteworthy that the overload of ROS induces accumulation of Aβ, establishing a vicious circle that reinforces the oxidative stress with strengthening of oxidative damage at neuronal level [33].

Based on these considerations, compound **12**, with a balanced inhibitory potency against these selected targets, together with a complete lack of toxic effects, might be considered a potential therapeutic agent to modify the course of AD.

7. Experimental section

7.1. Chemistry

Starting materials, unless otherwise specified, were used as high grade commercial products. Solvents were of analytical grade. Reaction progress was followed by thin layer chromatography (TLC) on precoated silica gel plates (Merck Silica Gel 60 F254) and then visualized with a UV254 lamplight. Chromatographic separations were performed on silica gel columns by flash method (Kieselgel 40, 0.040–0.063 mm, Merck). Melting points were determined in open glass capillaries, using a Büchi apparatus and are uncorrected.

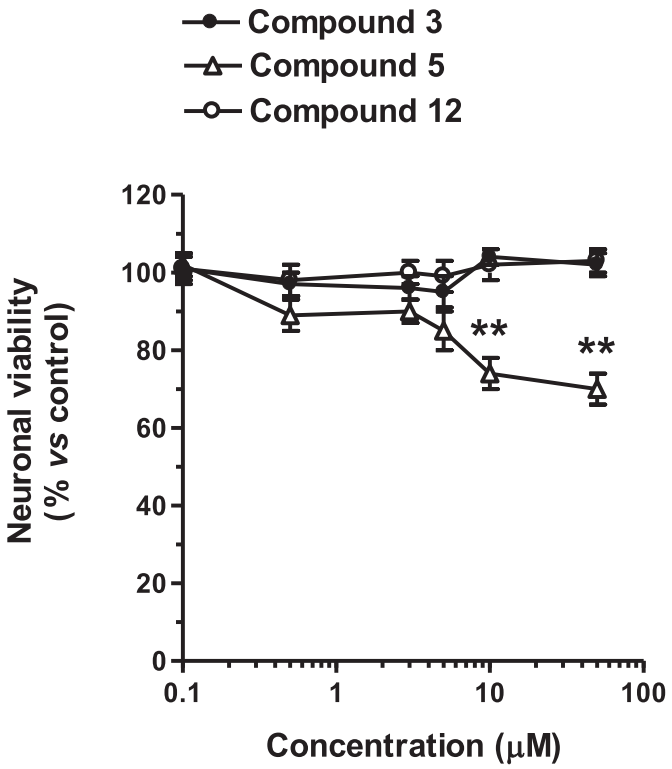

Fig. 4. Neurotoxicity of compounds **3**, **5** and **12** in SH-SY5Y cells. The neuronal viability in SH-SY5Y cells was determined by MTT assay (as described in the experimental section) after 24 h of incubation with various concentrations of compounds (0.1–50 μM). The results are expressed as a percentage of control cells and the values are reported as mean ± SD of three independent experiments (**$P < 0.01$ vs. cells treated with compound **3** at Student's *t*-test).

^{1}H NMR and ^{13}C NMR spectra were recorded on a Varian Gemini spectrometer 400 MHz, and chemical shifts (δ) are reported as parts per million (ppm) values relative to tetramethylsilane (TMS) as internal standard; coupling constants (J) are reported in Hertz (Hz). Standard abbreviations indicating spin multiplicities are given as follow: s (singlet), d (doublet), t (triplet), br (broad), q (quartet) or m (multiplet). Mass spectra were recorded on Waters ZQ 4000 apparatus operating in electrospray mode (ES). The purity of compounds was determined by elemental analysis; purity for all the tested compounds was superior to 95%. Compounds were named relying on the naming algorithm developed by CambridgeSoft Corporation and used in Chem-BioDraw Ultra 12.0.

7.2. General parallel procedure for the synthesis of compounds ***5***, ***7–15***

In distinct reactors the bromomethyl **18** (0.5 mmol, 0.15 g) was dissolved in toluene (5 mL), then the selected amine (0.75 mmol) and Et_3N (0.75 mmol) were added to the corresponding reactors. The mixtures were stirred under reflux for 12–20 h while monitoring with TLC. Purification of the crudes was achieved by flash chromatography on silica gel.

7.2.1. 4-(benzylmethylaminomethylphenyl)-3-fluoro-4-hydroxyphenylmethanone *5*

Reaction of **18** (0.5 mmol) and *N,N'*-benzylmethylamine (0.096 g) gave the crude final product **5** that was purified by flash chromatography (CH_2Cl_2/CH_3OH/NH_4OH 9.5/0.5/0.1). Yield 65%; brown semisolid. ^{1}H NMR ($CDCl_3$): δ 2.65 (s, 3H, N–CH_3), 4.04 (s, 2H, CH_2–N), 4.30 (s, 2H, CH_2–N), 7.00 (m, 1H, H-2), 7.47–7.64 (m, 3H, H-5, H-5′ and H-3′), 7.90–7.95 (m, 5H, phenyl), 7.98 (d, J = 8.6 Hz, 2H, H-2′ and H-6′), 8.35 (d, J = 8.6 Hz, 1H, H-6). ^{13}C NMR ($CDCl_3$): δ 55.25, 59.35, 60.32, 61.82, 112.17, 112.42, 117.82, 120.52, 127.48, 128.67, 129.78, 130.43, 130.48, 132.88, 136.31, 143.95, 147.29, 148.75, 150.47, 151.37, 151.48, 152.93, 170.15. ESI-MS (m/z): 350 ($M + H^+$).

7.2.2. 3-Fluoro-4-hydroxyphenyl-4-(3-hydroxybenzyl) methylaminomethylphenylmethanone *7*

Reaction of **18** (0.5 mmol) and 3-methylaminomethylphenol (0.097 g) gave the crude final product **7** that was purified by flash chromatography (CH_2Cl_2/CH_3OH/NH_4OH 9/1/0.1). Yield 75%, yellowish solid, mp 135–137 °C (AcOEt/*n*-hexane). ^{1}H NMR (DMSO): δ 2.55 (s, 3H, N–CH_3), 3.77 (s, 2H, CH_2–N), 3.79 (s, 2H, CH_2–N), 6.66 (dd, J = 1.8 and 8.6 Hz, 1H, H-4″), 6.87 (d, J = 8.6 Hz, 1H, H-6″), 6.90 (s, 1H, H-2″), 7.03–7.15 (m, 2H, H-2 and H-5″), 7.43 (d, J = 8.6 Hz, 1H, H-5), 7.51–7.58 (m, 3H, H-6, H-5′ and H-3′), 7.75 (d, J = 8.6 Hz, 2H, H-2′ and H-6′). ^{13}C NMR (DMSO): δ 58.28, 59.88, 62.33, 63.83, 111.12, 111.92, 115.81, 121.11, 125.32, 128.67, 129.78, 130.39, 130.42, 132.78, 135.99, 144.55, 147.29, 148.75, 151.47, 151.77, 152.54, 154.12, 170.33. ESI-MS (m/z): 366 ($M + H^+$).

7.2.3. 3-Fluoro-4-hydroxyphenyl-4-(2-hydroxyethyl) methylaminomethylphenylmethanone *8*

Reaction of **18** (0.5 mmol) and 2-methylaminoethanol (0.054 g) gave the crude final product **8** that was purified by flash chromatography (CH_2Cl_2/CH_3OH/NH_4OH 9.0/1.0/0.1). Yield 64%; white solid, mp 65–67 °C (AcOEt/*n*-hexane). ^{1}H NMR ($CDCl_3$): δ 2.30 (s, 3H, N–CH_3), 2.65 (t, J = 5.8 Hz, 2H, CH_2–N), 3.66 (t, J = 5.8 Hz, 2H, CH_2OH), 3.68 (s, 2H, CH_2–N), 4.99 (br, 1H, OH), 7.14 (t, J = 8.4 Hz, 1H, H-2), 7.42 (d, J = 8.4 Hz, 2H, H-3′ and H-5′), 7.51 (d, J = 8.4 Hz, 1H, H-5), 7.60 (dd, J = 1.8 and 8.4 Hz, 1H, H-6), 7.70 (d, J = 8.4 Hz, 2H, H-2′ and H-6′). ^{13}C NMR (acetone-d_6): δ 40.93, 58.35, 58.50, 61.02, 116.60, 116.66, 116.84, 127.03, 127.98, 128.66, 136.05, 142.81, 147.99, 149.26, 149.52, 152.82, 192.39. ESI-MS (m/z): 304 ($M + H^+$).

7.2.4. Fluoro-4-hydroxyphenyl-4-(4-hydroxypiperidin-1-ylmethyl) phenylmethanone *9*

Reaction of **18** (0.5 mmol) and piperidin-4-ol (0.078 g) gave the crude final product **9** that was purified by flash chromatography (CH_2Cl_2/CH_3OH/NH_4OH 9.0/1.0/0.1). Yield 83%; white solid, mp 66–69 °C (AcOEt/*n*-hexane). ^{1}H NMR (acetone-d_6): δ 1.54–1.65 (m, 2H, piperidine), 1.83–1.94 (m, 2H, piperidine), 2.08–2.33 (m, 2H, piperidine), 2.60–2.90 (m, 2H, piperidine), 3.30 (s, 2H, CH_2–N), 3.63–3.66 (m, 1H, piperidine), 4.26 (br, 1H, OH), 7.18 (t, J = 8.4 Hz, 1H, H-2), 7.42–7.58 (m, 4H, H-5, H-6, H-3′, H-5′), 7.82 (d, J = 8.4 Hz, 2H, H-2′, H-6′). ^{13}C NMR (acetone-d_6): δ 32.96, 50.07, 61.01, 65.54, 107.31, 117.39, 117.93, 128.25, 128.35, 128.89, 129.65, 133.16, 141.22, 151.23, 151.51, 219.29. ESI-MS (m/z): 330 ($M + H^+$).

7.2.5. 3-Fluoro-4-hydroxyphenyl-4-(4-phenylpiperazin-1-ylmethyl)phenylmethanone *10*

Reaction of **18** (0.5 mmol) and 1-phenylpiperazine (0.13 g) gave the crude final product **10** that was purified by flash chromatography (CH_2Cl_2/CH_3OH/NH_4OH 9.0/1.0/0.1). Yield 73%; white solid, mp 93–96 °C (AcOEt/*n*-hexane). ^{1}H NMR ($CDCl_3$): δ 2.68–2.77 (m, 4H, piperazine), 3.15–3.30 (m, 6H, CH_2–N and piperazine), 6.82–6.98 (m, 3H, phenyl), 7.14 (t, J = 8.4 Hz, 1H, H-2), 7.25–7.32 (m, 2H, phenyl), 7.49–7.61 (m, 4H, H-5, H-6, H-3′, H-5′), 7.77 (d, J = 8.4 Hz, 2H, H-2′, H-6′). ^{13}C NMR ($CDCl_3$): δ 45.22, 51.98, 53.68, 54.55, 62.28, 111.11, 117.45, 118.00, 127.02, 127.36, 128.60, 129.49, 129.50, 130.15, 130.25, 130.89, 131.65, 136.37, 137.02, 141.72, 150.50, 151.51, 194.29. ESI-MS (m/z): 391 ($M + H^+$).

7.2.6. 4-(4-Benzylpiperazin-1-ylmethyl)phenyl-3-fluoro-4-hydroxyphenylmethanone ***11***

Reaction of **18** (0.5 mmol) and 1-benzylpiperazine (0.13 g) gave the crude final product **11** that was purified by flash chromatography (CH_2Cl_2/CH_3OH/NH_4OH 9.5/0.5/0.1). Yield 78%; white solid, mp 101–103 °C (AcOEt/*n*-hexane). ^{1}H NMR ($CDCl_3$): δ 2.61–2.73 (m, 8H, piperazine), 3.58 (s, 2H, CH_2–N), 3.61 (s, 2H, CH_2–N), 6.94 (t, J = 8.4 Hz, 1H, H-2), 7.21–2.35 (m, 5H, phenyl), 7.40 (d, J = 8.4 Hz, 2H, H-3′, H-5′), 7.42–7.56 (m, 2H, H-5, H-6), 7.66 (d, J = 8.4 Hz, 2H, H-2′, H-6′). ^{13}C NMR ($CDCl_3$): δ 45.28, 52.00, 54.01, 54.15, 58.31, 62.55, 111.47, 117.21, 118.54, 127.72, 127.84, 128.11, 128.81, 129.13, 129.15, 129.25, 130.89, 131.65, 136.37, 137.02, 141.78, 150.12, 151.65, 195.46. ESI-MS (*m/z*): 405 ($M + H^+$).

7.2.7. 3-Fluoro-4-hydroxyphenyl-4-[4-(2-hydroxyethyl)piperidin-1-ylmethyl]phenylmethanone ***12***

Reaction of **18** (0.5 mmol) and 2-piperidin-4-ylethanol (0.125 g) gave the crude final product **12** that was purified by flash chromatography (CH_2Cl_2/CH_3OH/NH_4OH 9.5/0.5/0.1). Yield 78%; white solid (AcOEt/*n*-hexane), mp 101–103 °C; ^{1}H NMR ($CDCl_3$): δ 1.22–1.83 (m, 5H, piperidine), 2.04–2.13 (m, 2H, CH_2-piperidine), 2.90–3.05 (m, 4H, piperidine), 3.65 (t, J = 6.4 Hz, 2H, CH_2OH), 3.69 (s, 2H, CH_2–N), 5.12 (br, 1H, OH), 7.09 (t, J = 8.4 Hz, 1H, H-2), 7.43–7.57 (m, 4H, H-5, H-6, H-3′, H-5′), 7.76 (d, J = 8.4 Hz, 2H, H-2′, H-6′). ^{13}C NMR ($CDCl_3$): δ 25.11, 32.95, 50.09, 61.09, 65.59, 107.21, 117.39, 117.93, 128.25, 128.36, 128.88, 129.66, 133.12, 141.26, 151.26, 151.58, 219.27. ESI-MS (*m/z*): 405 ($M + H^+$).

7.2.8. 3-Fluoro-4-hydroxyphenyl-4-(4-methylpiperazin-1-ylmethyl)phenylmethanone ***13***

Reaction of **18** (0.5 mmol) and 1-methylpiperazine (0.13 g) gave the crude final product **13** that was purified by flash chromatography (CH_2Cl_2/CH_3OH/NH_4OH 9.5/0.5/0.1). Yield 74%; white solid, mp 88–89 °C (AcOEt/*n*-hexane). ^{1}H NMR ($CDCl_3$): δ 2.44 (s, 3H, CH_3), 2.56–2.69 (m, 8H, piperazine), 3.60 (s, 2H, CH_2), 6.91 (t, J = 8.4 Hz, 1H, H-2), 7.40 (d, J = 8.4 Hz, 2H, H-3′, H-5′), 7.46–7.56 (m, 2H, H-5, H-6), 7.68 (d, J = 8.4 Hz, 2H, H-2′, H-6′). ^{13}C NMR ($CDCl_3$): δ 29.16, 45.19, 51.92, 53.72, 54.55, 62.25, 111.46, 117.59, 118.03, 128.15, 128.25, 128.89, 129.65, 137.13, 147.72, 151.23, 151.51, 194.29. ESI-MS (*m/z*): 231 ($M + H^+$).

7.2.9. 4-(2-dimethylaminoethylmethylaminomethylphenyl)-3-fluoro-4-hydroxyphenylmethanone ***14***

Reaction of **18** (0.5 mmol) and N^1,N^1,N^2-trimethylethane-1,2-diamine (0.075 g) gave the crude final product **14** that was purified by flash chromatography (CH_2Cl_2/CH_3OH/NH_4OH 9.5/0.5/0.1). Yield 74%; white solid mp 73–75 °C (AcOEt/*n*-hexane). ^{1}H NMR ($CDCl_3$): δ 2.50 (s, 3H, CH_3), 2.89 (s, 6H, CH_3), 2.99 (t, J = 6.2 Hz, 2H, CH_2), 3.56 (t, J = 6.2 Hz, 2H, CH_2), 3.72 (s, 2H, CH_2), 4.09 (br, 1H, OH), 7.30 (t, J = 8.2 Hz, 1H, H-2), 7.46–7.56 (m, 4H, H-5, H-6, H-3′, H-5′), 7.65 (d, J = 8.4 Hz, 2H, H-2′, H-6′). ^{13}C NMR ($CDCl_3$): δ 40.93, 58.23, 58.35, 58.50, 67.02, 116.55, 116.58, 116.98, 127.54, 127.75, 128.88, 136.12, 142.41, 147.57, 149.32, 149.36, 152.24, 193.11. ESI-MS (*m/z*): 331 ($M + H^+$).

7.2.10. 4-Cyclohexylmethylaminomethylphenyl-3-fluoro-4-hydroxyphenylmethanone ***15***

Reaction of **18** (0.5 mmol) and *N*-methylcyclohexylamine (0.08 g) gave the crude final product **15** that was purified by flash chromatography (CH_2Cl_2/CH_3OH/NH_4OH 9.5/0.5/0.1). Yield 73%; white solid mp 65–67 °C (AcOEt/*n*-hexane). ^{1}H NMR (acetone-d_6): δ 1.20–1.41 (m, 6H, cyclohexane C-3, C-4, C-5), 1.75–1.98 (m, 4H, cyclohexane C-2, C-6), 2.21 (s, 3H, CH_3), 2.43–2.51 (m, 1H, cyclohexane C-1), 3.51 (s, 2H, CH_2), 4.90 (br, 1H, OH), 7.09 (t, J = 8.4 Hz, 1H, H-2), 7.65–7.68 (m, 4H, H-5, H-6, H-3′, H-5′), 7.73 (d, J = 8.4 Hz, 2H, H-2′, H-6′). ^{13}C NMR ($CDCl_3$): δ 22.11, 24.32, 24.36, 25.45, 25.89, 40.93, 43.12, 59.35, 59.65, 61.02, 116.60, 116.68, 116.88, 127.24, 127.47, 128.47, 136.35, 142.54, 147.27, 149.95, 149.99, 152.99, 191.16. ESI-MS (*m/z*): 342 ($M + H^+$).

7.3. General procedure for the synthesis of compounds ***6*** *and* ***18***

BBr_3 (1 M solution in CH_2Cl_2, 1.5 equiv) was added dropwise to a solution of the methoxy derivative (1 equiv) in anhydrous CH_2Cl_2 (2 mL), at 0 °C and under N_2 atmosphere. The solution was stirred for 2 h at the same temperature, then overnight at room temperature. The mixture was neutralized with $NaHCO_3$ saturated solution and then extracted with CH_2Cl_2, the combined organic layers were dried (Na_2SO_4) to afford a crude residue, which was purified by flash column chromatography.

7.3.1. 3-Fluoro-4-hydroxyphenyl-p-tolylmethanone ***6***

Reaction of **16** [19] gave the crude product **6** that was purified by flash chromatography (petroleum ether/AcOEt 9/1). Yield 71%; white solid, mp 100–101 °C. ^{1}H NMR ($CDCl_3$): δ 2.37 (s, 3H, CH_3), 4.50 (br, 1H, OH), 6.94 (t, J = 8.4 Hz, 1H, H-2), 7.21 (d, J = 8.4 Hz, 2H, H-3′, H-5′), 7.46–7.56 (m, 4H, H-2′, H-6′, H-5, H-6). ^{13}C NMR ($CDCl_3$): δ 21.50, 117.13, 117.19, 117.65, 118.04, 128.94, 129.87, 135.07, 148.50, 148.78, 149.07, 207.32. ESI-MS (*m/z*): 231 ($M + H^+$).

7.3.2. 4-bromomethylphenyl-3-fluoro-4-hydroxyphenylmethanone ***18***

Reaction of **17** [19] gave the crude product **18**, that was purified by flash column chromatography (petroleum ether/AcOEt 7/3). Yield 92%; white solid, mp 145–147 °C. ^{1}H NMR ($CDCl_3$): δ 4.53 (s, 2H, CH_2Br), 5.90 (br, 1H, OH), 7.08 (t, J = 8.4 Hz, 1H, H-2), 7.50 (d, J = 8.0 Hz, 2H, H-3′, H-5′), 7.59 (d, J = 8.0 Hz, 1H, H-5), 7.65–7.68 (m, 1H, H-6), 7.73 (d, J = 8.4 Hz, 2H, H-2′, H-6′).

7.4. BACE-1 inhibition. FRET inhibition assay

FRET inhibition studies were performed using the following procedures: 5 μL of test compound (or DMSO) were pre-incubated with 175 μL of BACE-1 (17.2 nM, final concentration) in 20 mM sodium acetate pH 4.5 containing CHAPS (0.1% w/v) for 1 h at room temperature. M-2420 (3 μM, final concentration) was then added and left to react for 15 min at 37 °C. The fluorescence signal was read at λ_{em} = 405 nm (λ_{exc} = 320 nm). DMSO concentration in the final mixture was maintained below 5% (v/v) to guarantee no significant loss of enzyme activity. Fluorescence intensities with and without inhibitors were registered and compared. The percent inhibition due to the presence of test compounds was calculated. The background signal was measured in control wells containing all the reagents, except hrBACE-1, and subtracted. The % inhibition due to the presence of test compound was calculated by the following expression: $100 - (IF_i/IF_o \times 100)$ where IF_i and IF_o are the fluorescence intensities obtained for hrBACE-1 in the presence and in the absence of inhibitor, respectively [28]. The linear regression parameters were determined and the IC_{50} interpolated (GraphPad Prism 4.0, GraphPad Software Inc.).

7.5. AChE inhibition

The capacity of compounds **5**, **7**–**15** to inhibit AChE activity was assessed by Ellman's method [29]. AChE stock solution was prepared by dissolving human recombinant AChE (E.C.3.1.1.7) lyophilized powder (Sigma, Italy) in 0.1 M phosphate buffer (pH = 8.0) containing Triton X-100 (0.1%). Five increasing concentrations of inhibitor were assayed to obtain % inhibition of the enzymatic activity in the range of 20–80. The assay solution consisted of a 0.1 M

phosphate buffer pH 8.0, with the addition of 340 μM 5,5′-dithiobis(2-nitrobenzoic acid), 0.02 unit/mL of human recombinant AChE from human serum and 550 μM of substrate (acetylthiocholine iodide, ATCh). Increasing concentrations of tested inhibitor were added to the assay solution and pre-incubated for 20 min at 37 °C with the enzyme followed by the addition of substrate. Initial rate assays were performed at 37 °C with a Jasco V-530 double beam Spectrophotometer. Absorbance value at 412 nm was recorded for 5 min and enzyme activity was calculated from the slope of the obtained linear trend. Assays were carried out with a blank containing all components except AChE to account for the non-enzymatic reaction. The reaction rates were compared and the percent inhibition due to the presence of tested inhibitors was calculated. Each concentration was analysed in duplicate, and IC_{50} values were determined graphically from log concentration–inhibition curves (GraphPad Prism 4.03 software, GraphPad Software Inc.).

7.6. Antioxidant activity and neurotoxicity in human neuronal SH-SY5Y cells

7.6.1. Chemicals

$A\beta_{25-35}$ peptide, 3-(4,5-dimethyl-2-thiazolyl)-2,5-diphenyl-2H-tetrazolium bromide (MTT), dihydroethidium (DHE) and tert-butylhydroperoxide (*t*-BuOOH) were purchased from Sigma Chemical Co. All other reagents were of the highest grade of purity commercially available.

7.6.2. Cell cultures

Human neuronal (SH-SY5Y) cells were routinely grown in Dulbecco's modified Eagle' medium supplemented with 10% fetal bovine serum, 2 mM glutamine, 50 U mL^{-1} penicillin, and 50 μg mL^{-1} streptomycin at 37 °C in a humidified incubator with 5% CO_2.

7.6.3. Determination of neurotoxicity induced by compounds

To evaluate the neurotoxic effects of compounds, the SH-SY5Y cells were seeded in 96-well plates at 2×10^4 cells/well, incubated for 24 h and subsequently treated with various concentrations of compounds (0.1–50 μM). The neuronal viability in terms of mitochondrial metabolic function was evaluated by the reduction of MTT to formazan as previously described [38]. Briefly, the treatment medium was replaced with MTT (5 mg/mL) in phosphate buffered saline (PBS) for 2 h at 37 °C in 5% CO_2. After washing with PBS, the formazan crystals were dissolved with isopropanol. The amount of formazan was measured (570 nm, ref. 690 nm) with a spectrophotometer (TECAN®, GENios, Salzburg, Austria). The neuronal viability is expressed as a percentage of control cells.

7.6.4. Determination of t-BuOOH-induced intracellular ROS formation

The intracellular ROS formation induced by *t*-BuOOH at SH-SY5Y cell level was determined using DHE (λ_{exc} = 380 nm, λ_{em} = 445 nm). Briefly, SH-SY5Y cells were cultured in 96-well microtiter plates at 3×10^4 cells/well for 24 h. The medium was then removed and the cells were washed with PBS and then incubated with DHE (10 μM) in PBS for 30 min in the dark. After removal of the probe and further washing, the cells were co-treated with various concentrations of compounds (0.5–5 μM) and *t*-BuOOH (100 μM) for 30 min at room temperature in the dark. At the end of incubation, the red fluorescence of the cells from each well was measured with a spectrofluorometer (TECAN®, GENios). The results are expressed as fold increase of intracellular ROS evoked by exposure to *t*-BuOOH.

7.6.5. $A\beta_{25-35}$ peptide preparation for intracellular ROS formation assay

$A\beta_{25-35}$ peptides were first dissolved in hexafluoroisopropanol to 1 mg mL^{-1}, sonicated, incubated at room temperature for 24 h and lyophilized. The resulting unaggregated $A\beta_{25-35}$ peptide film was dissolved with dimethylsulfoxide and stored at −20 °C until use.

7.6.6. Determination of $A\beta_{25-35}$ peptide-induced intracellular ROS formation

The intracellular ROS formation induced by $A\beta_{25-35}$ peptides at SH-SY5Y cell level was determined using the probe DHE as previously described [39]. Briefly, SH-SY5Y cells were cultured in BD Falcon™ 8-well Culture slides (surface area 0.7 cm^2/well) at 1×10^4 cells/well for 24 h. The cells were then co-treated with various concentrations of compounds (0.5–5 μM) and $A\beta_{25-35}$ peptides (5 μM). At the end of treatment, the cells were washed and incubated with DHE (10 μM) in PBS for 30 min in the dark. After removal of the probe, cells were washed with PBS and incubated with DMEM serum free for 1 h at 37 °C. Intracellular ROS formation was measured under a fluorescence microscope (Zeiss Axio Imager M1). Fluorescence images were captured with an AxioVision image recording system computer. Four randomly selected areas with 50–100 cells in each were analysed and the values obtained are expressed as fold increases of ROS formation vs. untreated cells.

7.6.7. Statistical analysis

Data are reported as mean ± SD of at least 3 independent experiments. Statistical analysis was performed using one-way ANOVA with the Dunnett post hoc test and Student's *t*-test, as appropriate. Differences were considered significant at $p < 0.05$. Analyses were performed using GraphPad Prism 4.0 software.

7.7. Molecular docking

The docking simulations were carried out by means of ICM 3.7 [40]. The protein structure was prepared starting from the crystallographic complex of BACE-1 2ZJM [31]. Hydrogen atoms were added. Polar hydrogen atoms, and the positions of asparagine and glutamine side chain amidic groups were optimized and assigned the lowest energy conformation. After optimization, histidines were automatically assigned the tautomerization state that improved the hydrogen bonding pattern. Ligands were built defining the right bond orders, stereochemistry, hydrogen atoms, and protonation states. Each ligand was assigned the MMFF force field atom types and charges [41]. The residues with at least one heavy atom within 5 Å from the bound conformation of the co-crystallized inhibitors were considered to define the boundaries of the binding box. The docking engine employed was the Biased Probability Monte Carlo (BPMC) stochastic optimizer as implemented in ICM [42]. The ligand binding site at the receptor was represented by pre- calculated 0.5 Å spacing potential grid maps, representing van der Waals potentials for hydrogens and heavy probes, electrostatics, hydrophobicity, and hydrogen bonding. The van der Waals inter-actions were described by a smoother form of the 6–12 Lennard-Jones potential with the repulsive contribution capped at 4.0 kcal/mol. The electrostatic contribution was buffered, artificially increasing the distance between oppositely charged atoms in order to avoid their collapse when the electrostatic attractive energy prevailed on the softened van der Waals repulsion. The molecular conformation was described by means of internal coordinate variables. The adopted force field was a modified version of the ECEPP/3 force field with a distance-dependent dielectric constant [43]. Given the number of rotatable bonds in the ligand, the basic number of BPMC steps to be carried out was

calculated by an adaptive algorithm (thoroughness 1.0). The binding energy was assessed by means of the standard ICM empirical scoring function [44].

Appendix A. Supplementary data

Supplementary data related to this article can be found at http://dx.doi.org/10.1016/j.ejmech.2014.03.042.

References

[1] J.L. Cummings, Alzheimers Dement 5 (2009) 406–418.
[2] A. Cavalli, M.L. Bolognesi, A. Minarini, M. Rosini, V. Tumiatti, M. Recanatini, C. Melchiorre, Journal of Medicinal Chemistry 51 (2008) 347–372.
[3] J. Hardy, D.J. Selkoe, Science 297 (2002) 353–356.
[4] J.A. Hardy, G.A. Higgins, Science 256 (1992) 184–185.
[5] D.A. Butterfield, J. Drake, C. Pocernich, A. Castegna, Trends in Molecular Medicine 7 (2001) 548–554.
[6] D.A. Butterfield, A.M. Swomley, R. Sultana, Antioxidants & Redox Signaling 19 (2013) 823–835.
[7] J. Hardy, Journal of Alzheimer's Disease 9 (2006) 151–153.
[8] M.A. Smith, P.L. Harris, L.M. Sayre, G. Perry, Proceedings of the National Academy of Sciences of the United States of America 94 (1997) 9866–9868.
[9] P.H. Reddy, M.F. Beal, Trends in Molecular Medicine 14 (2008) 45–53.
[10] D. Pratico, Trends in Pharmacological Sciences 29 (2008) 609–615.
[11] E. Tamagno, P. Bardini, A. Obbili, A. Vitali, R. Borghi, D. Zaccheo, M.A. Pronzato, O. Danni, M.A. Smith, G. Perry, M. Tabaton, Neurobiology of Disease 10 (2002) 279–288.
[12] X. Zhang, K. Zhou, R. Wang, J. Cui, S.A. Lipton, F.F. Liao, H. Xu, Y.W. Zhang, Journal of Biological Chemistry 282 (2007) 10873–10880.
[13] M. Guglielmotto, M. Aragno, R. Autelli, L. Giliberto, E. Novo, S. Colombatto, O. Danni, M. Parola, M.A. Smith, G. Perry, E. Tamagno, M. Tabaton, Journal of Neurochemistry 108 (2009) 1045–1056.
[14] L. Chami, V. Buggia-Prevot, E. Duplan, D. Delprete, M. Chami, J.F. Peyron, F. Checler, Journal of Biological Chemistry 287 (2012) 24573–24584.
[15] E. Tamagno, M. Guglielmotto, D. Monteleone, M. Tabaton, Neurotoxicity Research 22 (2012) 208–219.
[16] R. Silvestri, Medicinal Research Reviews 29 (2009) 295–338.
[17] L. Hong, G. Koelsch, X. Lin, S. Wu, S. Terzyan, A.K. Ghosh, X.C. Zhang, J. Tang, Science 290 (2000) 150–153.
[18] W.H. Huang, R. Sheng, Y.Z. Hu, Current Medicinal Chemistry 16 (2009) 1806–1820.
[19] S.A. Hitchcock, L.D. Pennington, Journal of Medicinal Chemistry 49 (2006) 7559–7583.
[20] V. John, Current Topics in Medicinal Chemistry 6 (2006) 569–578.
[21] G. La Regina, F. Piscitelli, R. Silvestri, Journal of Heterocyclic Chemistry 46 (2009) 10–17.
[22] B.E. Evans, K.E. Rittle, M.G. Bock, R.M. DiPardo, R.M. Freidinger, W.L. Whitter, G.F. Lundell, D.F. Veber, P.S. Anderson, R.S. Chang, et al., Journal of Medicinal Chemistry 31 (1988) 2235–2246.
[23] R.W. DeSimone, K.S. Currie, S.A. Mitchell, J.W. Darrow, D.A. Pippin, Combinatorial Chemistry & High Throughput Screening 7 (2004) 473–494.
[24] F. Belluti, L. Piazzi, A. Bisi, S. Gobbi, M. Bartolini, A. Cavalli, P. Valenti, A. Rampa, European Journal of Medicinal Chemistry 44 (2009) 1341–1348.
[25] F. Belluti, M. Bartolini, G. Bottegoni, A. Bisi, A. Cavalli, V. Andrisano, A. Rampa, European Journal of Medicinal Chemistry 46 (2011) 1682–1693.
[26] L. Piazzi, A. Cavalli, F. Colizzi, F. Belluti, M. Bartolini, F. Mancini, M. Recanatini, V. Andrisano, A. Rampa, Bioorganic & Medicinal Chemistry Letters 18 (2008) 423–426.
[27] W.K. Hagmann, Journal of Medicinal Chemistry 51 (2008) 4359–4369.
[28] F. Mancini, A. De Simone, V. Andrisano, Analytical and Bioanalytical Chemistry 400 (2011) 1979–1996.
[29] G.L. Ellman, K.D. Courtney, V. Andres Jr., R.M. Feather-Stone, Biochemical Pharmacology 7 (1961) 88–95.
[30] A. Rauk, Dalton Transactions (2008) 1273–1282.
[31] W. Yang, R.V. Fucini, B.T. Fahr, M. Randal, K.E. Lind, M.B. Lam, W. Lu, Y. Lu, D.R. Cary, M.J. Romanowski, D. Colussi, B. Pietrak, T.J. Allison, S.K. Munshi, D.M. Penny, P. Pham, J. Sun, A.E. Thomas, J.M. Wilkinson, J.W. Jacobs, R.S. McDowell, M.D. Ballinger, Biochemistry 48 (2009) 4488–4496.
[32] B. Turk, Nature Reviews Drug Discovery 5 (2006) 785–799.
[33] E. Tamagno, M. Guglielmotto, M. Aragno, R. Borghi, R. Autelli, L. Giliberto, G. Muraca, O. Danni, X. Zhu, M.A. Smith, G. Perry, D.G. Jo, M.P. Mattson, M. Tabaton, Journal of Neurochemistry 104 (2008) 683–695.
[34] H. Pajouhesh, G.R. Lenz, NeuroRx 2 (2005) 541–553.
[35] M.C. Wenlock, R.P. Austin, P. Barton, A.M. Davis, P.D. Leeson, Journal of Medicinal Chemistry 46 (2003) 1250–1256.
[36] J. Tang, A. Ghosh, Aging (Albany NY) 3 (2011) 14–16.
[37] A.K. Ghosh, M. Brindisi, J. Tang, Journal of Neurochemistry 120 (Suppl. 1) (2012) 71–83.
[38] A. Tarozzi, A. Merlicco, F. Morroni, C. Bolondi, P. Di Iorio, R. Ciccarelli, S. Romano, P. Giuliani, P. Hrelia, Journal of Biology Regulators and Homeostatic Agents 24 (2010) 297–306.
[39] S. Rizzo, A. Tarozzi, M. Bartolini, G. Da Costa, A. Bisi, S. Gobbi, F. Belluti, A. Ligresti, M. Allara, J.P. Monti, V. Andrisano, V. Di Marzo, P. Hrelia, A. Rampa, European Journal of Medicinal Chemistry 58 (2012) 519–532.
[40] R. Abagyan, A. Orry, E. Raush, M. Totrov, ICM Manual 3.7, Molsoft LCC, La Jolla, CA, 2013.
[41] T.A. Halgren, R.B. Nachbar, Journal of Computational Chemistry 17 (1996) 587–615.
[42] R.T. Abagyan, Journal of Molecular Biology 235 (1994) 983–1002.
[43] G. Nemethy, K.D. Gibson, K.A. Palmer, C.N. Yoon, G. Paterlini, A. Zagari, S. Rumsey, H.A. Scheraga, Journal of Physical Chemistry 96 (1992) 6472–6484.
[44] M.A. Totrov, in: Drug-receptor Thermodynamics: Introduction and Applications, 2001, pp. 603–624.
[45] S. Rizzo, A. Bisi, M. Bartolini, F. Mancini, F. Belluti, S. Gobbi, V. Andrisano, A. Rampa, European Journal of Medicinal Chemistry 46 (2011) 4336–4343.